

## Magnetism of the Ni(110) and Ni(100) surfaces: Local-spin-density-functional calculations using the thin-slab linearized augmented-plane-wave method

H. Krakauer

*Department of Physics, College of William and Mary, Williamsburg, Virginia 23185*

A. J. Freeman

*Department of Physics, Northwestern University, Evanston, Illinois 60201  
and Argonne National Laboratory, Argonne, Illinois 60439*

E. Wimmer\*

*Department of Physics, Northwestern University, Evanston, Illinois 60201*

(Received 24 February 1983)

Results of self-consistent local-spin-density-functional calculations are reported for the first time for the Ni(110) surface, represented by one-, three-, and five-layer slabs. Calculations for one- and five-layer slabs of Ni(100) are also reported. The behavior of the surface magnetization with varying slab thickness elucidates the nature and origin of the surface magnetic moment. We predict a 13% *enhancement* of the Ni(110) surface magnetic moment compared to the bulk value. For the Ni(100) surface, we find a smaller surface *enhancement* about 7%, compared to bulk, which agrees with the results of Jepsen *et al.* The enhancement of surface magnetic moments on Ni(100) and Ni(110) surfaces is attributed to *s-d* dehybridization at the surface and to the presence of electrostatic shifts required to maintain layer-by-layer charge neutrality. We find that the *total d*-electron charge is the same in each layer, which contradicts the *sp-to-d* charge transfer found by Tersoff and Falicov at transition-metal surfaces. An exchange-split pair of very localized surface states is found on the Ni(110) surface, which is in good agreement with the photoemission measurements of Eberhardt *et al.* The theoretical exchange splitting, 0.6 eV, is twice as large as that found experimentally. This discrepancy is similar to that found for the bulk Ni bands and is attributed to neglected many-body effects. For Ni(100) it is found that surface states at the Brillouin-zone center are unable to account for the reversal above threshold of the spin polarization of photoemitted electrons, in agreement with other self-consistent calculations. A majority-spin  $\bar{\Sigma}_2$  surface resonance on Ni(100) is in good agreement with the experimental surface state of Plummer and Eberhardt but has greater dispersion downward away from the Fermi energy than is found experimentally. We do not find the  $\bar{\Delta}_1$  minority-spin surface-state band observed by Plummer and Eberhardt just below the Fermi energy; instead, we find a flat  $\bar{\Delta}_2$  minority-spin surface-state band about 0.5 eV below the Fermi energy. Finally, we find surface core-level chemical shifts to reduced binding energy of 0.39 eV on Ni(100) and 0.45 eV on Ni(110). The polarization of the core states by the valence electrons splits the spin-up and spin-down core states in each layer by about 0.6 eV, thereby permitting, in principle at least, the experimental verification of these surface core-level shifts, since the two spin manifolds are separated.

### I. INTRODUCTION

The study of the magnetism of surfaces and interfaces represents part of a general increase in interest in transition-metal materials on the microstructure scale. The unique chemical and physical properties of transition metals play an especially important role in determining the observable phenomena in such reduced-symmetry systems as small particles (or clusters of atoms), surfaces, interfaces, and modulated structures. Fortunately for the theoretical treatment of these problems, the theory of itinerant-electron magnetism has been considerably advanced in recent years by the success of local-density and local-spin-density *ab initio* self-consistent band-theory calculations in providing a quantitative understanding of many ground-state properties of the ferromagnetic transition metals, iron, cobalt, and nickel.<sup>1-4</sup> These calculations have been remarkably successful in obtaining good agreement with such experimental quantities as magneti-

zation, neutron form factors, hyperfine field, lattice parameter, bulk modulus, cohesive energies, and Fermi-surface properties. This is particularly impressive, considering that all many-electron effects are included only through an effective one-electron local potential. This achievement is a major confirmation of the utility of Hohenberg-Kohn-Sham<sup>5</sup> local- (spin-<sup>6-8</sup>) density-functional theory which provides the formal justification for using the single-particle picture to determine ground-state properties. While the ground-state properties are now quantitatively understood on this basis,<sup>1</sup> this is not true, unfortunately, for the elementary excitations and temperature-dependent effects of itinerant-electron ferromagnets,<sup>9</sup> although there have been significant advances in these areas in recent years.<sup>10-23</sup>

Spin-density-functional theory provides the formal justification for using single-particle band structures and charge densities to obtain ground-state properties only. There is, however, no formal sanction to interpret the

band structure in terms of effective independent-quasiparticle states,<sup>13–23</sup> although the agreement (especially in metals) is sometimes surprisingly good. Of the three ferromagnetic elements, the limitations of local-spin-density-functional (LSDF) theory are most apparent in Ni<sup>24</sup> where photoemission experiments<sup>24–27</sup> map out energy bands which differ considerably from those predicted by theory.<sup>3</sup>

On the experimental side, the past few years have witnessed major advances in the use of angle-resolved photoemission<sup>24–27</sup> and such novel techniques as electron capture spectroscopy,<sup>28</sup> spin-polarized low-energy electron diffraction (LEED),<sup>29</sup> and inverse photoemission.<sup>30</sup> New and remarkably detailed information on the ferromagnetic transition metals (especially from photoemission) have thus provided a well-charted area for testing the limitations of the single-particle picture and our understanding of the important many-body processes. Many of the experimental methods such as photoemission, however, are intrinsically surface sensitive, and the experimentally observed features may involve bulk effects and/or surface effects such as the possible existence of magnetically “dead” surface layers<sup>31–34</sup> and magnetic surface states.<sup>35–37</sup> These surface effects are interrelated as demonstrated by the recent photoemission observation<sup>36</sup> of exchange-split surface states (with temperature-dependent exchange splitting) on the Ni(110) surface. Unless these states are well localized in the surface layer, however, the possibility of “dead layers” for this surface could not be ruled out. As shown in Sec. III of this paper, these states are indeed extremely localized in the surface layer. Taken together, the good agreement between experiment<sup>36</sup> and our theoretical results for this surface state provide very strong evidence for the presence of surface magnetism on Ni(110). The absence of dead layers is also supported by recent spin-polarized LEED experiments<sup>29</sup> on the Ni(110) surface. The photoelectron-spin-polarization reversal<sup>38–44</sup> observed just above threshold in Ni is another example where surface effects (surface states and unbound evanescent states) have been suggested<sup>38,39</sup> to play a decisive role.

There has, therefore, been great interest in the past few years in the electronic structure of ferromagnetic metal surfaces. Exchange-split surface states have been mapped out on the Ni(100) surface by Plummer and Eberhardt<sup>35</sup> and by Erskine.<sup>37</sup> Some of these states had been predicted previously to exist in the non-self-consistent calculations of Dempsey and Kleinman.<sup>38</sup> As mentioned, prominent exchange-split surface states were also observed by Eberhardt *et al.*<sup>36</sup> on the Ni(110) surface and used to rule out magnetically dead surface layers, and these states have been found for the first time in the linearized-augmented-plane-wave (LAPW) calculations presented here.

A related area of interest is the magnetic properties of very thin ferromagnetic overlayers on nonmagnetic substrates.<sup>28,31–34</sup> Liebermann *et al.*<sup>31</sup> observed magnetically dead layers for less than about 2.5 layers of Ni deposited on a Cu substrate. Anomalous Hall-effect measurements by Bergmann<sup>33</sup> confirmed the existence of dead layers, but the spin-polarized photoemission measurements of Pierce and Siegmann<sup>32</sup> suggest that Ni becomes ferromagnetic for overlayer thickness as low as a monolayer. Similarly, electron-capture spectroscopy measurements<sup>28</sup> find that a Ni monolayer on Cu is not magnetically dead but has a re-

duced moment. Self-consistent thin-film calculations of Ni overlayers on a Cu(100) substrate<sup>45</sup> have found that even one monolayer of Ni on Cu is not magnetically dead (the moment is reduced to  $0.39\mu_B$ ).

Compared to the number of bulk calculations, there have been only a handful of such studies for surfaces<sup>45</sup> and other reduced-symmetry systems.<sup>46,47</sup> Wang and Freeman<sup>48</sup> performed self-consistent linear combination of atomic orbitals discrete-variational method (LCAO-DVM) calculations for a nine-layer slab of Ni(100). In these pioneering calculations they found that the surface was not magnetically dead, but that the surface-layer magnetic spin moment was reduced by 20% from the center layer which had the bulk value. They attributed this effect to the presence of a majority-spin *d*-hole surface state just above the Fermi energy, at the corner of the Brillouin zone (BZ) (the  $\bar{M}$  point). They also found surface states at the center of the BZ ( $\bar{\Gamma}$ ) 0.24 eV below  $E_F$  (a  $\bar{\Gamma}_5$  state) and 0.33 eV below  $E_F$  (a  $\bar{\Gamma}_4$  state). In an earlier non-self-consistent parametrized calculation, Dempsey and Kleinman<sup>38</sup> found these majority-spin surface states to be highly localized in the surface layer, and they claimed that emission from these states into an unbound evanescent state accounts for the reversal of photoelectron-spin polarization observed 0.1 eV above threshold. The surface states found by Wang and Freeman, on the other hand, are not sufficiently localized in the surface layers to account for the polarization reversal. Wang and Freeman also found Friedel oscillations in the spin density of their nine-layer slab and suggested that these would be missed in slabs as thin as five layers, thus raising the important question of possible size effects. A possibly serious shortcoming was that self-consistency was achieved in this LCAO-DVM calculation by fitting the true charge density in each iteration to a superposition of spherically symmetric atomic charge densities (the fitting parameters were the noninteger *s*, *p*, and *d* atomic occupation numbers for each inequivalent atom). Since the true charge density cannot be expanded strictly in terms of only spherically symmetric single-site functions, this procedure might affect the accuracy of the charge density and the resulting potential, especially in the more open surface regions. Although this procedure probably describes the overall charge-transfer features, it may have more significant effects on such sensitive quantities as the magnetization and surface states.

Jepsen *et al.*<sup>49</sup> also presented results of a spin-polarized calculation, but for a five-layer Ni(001) slab. They also found that the surface was not magnetically dead, but they reported a slight *increase* in the surface magnetic moment. Their values were  $0.61\mu_B$ ,  $0.55\mu_B$ , and  $0.58\mu_B$  per atom in the surface, subsurface, and central layers, respectively. They used a version of LAPW which differs significantly from that used in the present paper, notably, the procedure for synthesizing and using (i) the nonspherical muffin-tin potential components, and (ii) the nonplanar averaged vacuum potential components. In both cases, the additional approximation is made by using the continuation of the interstitial plane-wave LAPW basis function into these regions rather than the exact form of the LAPW basis function. In addition, the corresponding Hamiltonian matrix elements are then calculated, also using the plane-wave continuation of the basis function.

While there is some justification for these approximations, they are essentially uncontrolled, and it is difficult to predict their effect when iterating to self-consistency.

In this paper we present results of LSDF self-consistent calculations on one-, three-, and five-layer Ni(110) slabs and on one- and five-layer Ni(100) slabs, using our thin-film LAPW<sup>50,51</sup> method. This approach treats the full spatial variation of the potential everywhere in the interstitial and vacuum regions but neglects the nonspherical components of the potential inside the muffin-tin spheres. The organization of this paper is as follows. Section II gives the details of the self-consistent LAPW method used; Sec. III presents the results of our calculations and compares them to other calculations and experiments; Sec. IV contains our principal conclusions.

## II. METHODOLOGY

We employ the self-consistent LAPW film method<sup>50,51</sup> as generalized to deal with spin polarization. The spin-dependent exchange-correlation potential  $V_{xc}$  of von Barth and Hedin<sup>6</sup> is used in the LSDF formalism to determine the electronic energy-band structure,

$$V_{xc}^{\alpha} = A(\rho)(2\rho^{\alpha}/\rho)^{1/3} + B(\rho), \quad (1)$$

where  $\rho^{\alpha} = \rho^{\uparrow}$  or  $\rho^{\downarrow}$  and  $\rho = \rho^{\uparrow} + \rho^{\downarrow}$  denote the spin-up or spin-down and the total electron density, respectively. The  $A$  and  $B$  coefficients are given by<sup>6</sup>

$$A(\rho) = \mu_x^p(\rho) + v_c(\rho),$$

$$B(\rho) = \mu_c^p(\rho) - v_c(\rho).$$

Here

$$\mu_x^p(\rho) = -(3/\pi)^{1/3} \rho^{1/3}$$

and

$$\mu_c^p(\rho) = -c^p \ln[1 + (4\pi/3)^{1/3} r^p \rho^{1/3}]$$

are the contribution of exchange and correlation to the chemical potential, and

$$v_c(\rho) = -\frac{4}{3} \frac{1}{2^{1/3} - 1} \left[ c^f F \left[ \frac{1}{(4\pi/3)^{1/3} r^f \rho^{1/3}} \right] - c^p F \left[ \frac{1}{(4\pi/3)^{1/3} r^p \rho^{1/3}} \right] \right],$$

with the function

$$F(z) \equiv (1+z^3) \ln(1+1/z) + \frac{1}{2}z - z^2 - \frac{1}{3}.$$

The coefficients  $c^f$  and  $r^f$  are set equal to  $c^p/2$  and  $2^{4/3}r^p$ , respectively, according to scaling suggested by the random-phase approximation,<sup>6</sup> and  $c^p=0.045$  and  $r^p=21.0$  are chosen to yield the paramagnetic correlation term of Hedin and Lundqvist.<sup>52</sup>

The core charge density ( $1s^2 2s^2 2p^6 3s^2 3p^6$ ) is computed using a fully relativistic Dirac-Slater-type atomic-structure program, while for the valence electrons only a semirelativistic<sup>53</sup> computation (without spin-orbit coupling) is used. All states, including the core states, are computed self-consistently for every iteration. This is important for the accurate calculation of the surface core-

level shifts. The treatment of spin polarization for the core states deserves some comment. The majority-spin and minority-spin core charge density in a given iteration are obtained from the current spin-up and spin-down muffin-tin potentials in that iteration. With the inclusion of spin-orbit coupling for the core, however, spin is no longer a good quantum number, and this approach is strictly not correct. We believe, however, that our procedure is essentially equivalent to (i) first obtaining spin-polarized *scalar-relativistic* core-state solutions for the spin-up and spin-down potentials, and (ii) then including the spin-orbit interaction in a second variational step.

In the interstitial and vacuum regions, the full potential without any shape approximation is determined self-consistently and included in the computations while nonspherical terms are neglected inside the muffin-tin spheres. The Coulomb potential is obtained by a very accurate solution of Poisson's equation<sup>51</sup> permitting a very precise determination of the potential near the surface region, thus giving a good description of the surface states and surface electronic properties.

Calculations were performed for ideal (e.g., no relaxation) one- to five-layer Ni(100) and Ni(110) slabs. As found for the W(001) surface,<sup>54</sup> the electronic structure is not expected to be very sensitive to small (5%) relaxations of the surface atoms. Therefore the approximation of using the bulk bond distances for the surface atoms also is believed to be a good one in the present calculations. For the systems under consideration, the basis size is about 55 LAPW's per atom resulting in eigenvalues which are converged to better than about 3 mRy. Fifteen  $\bar{k}$  points in the irreducible wedge (Fig. 1) of the two-dimensional BZ are used to generate the charge density in the self-

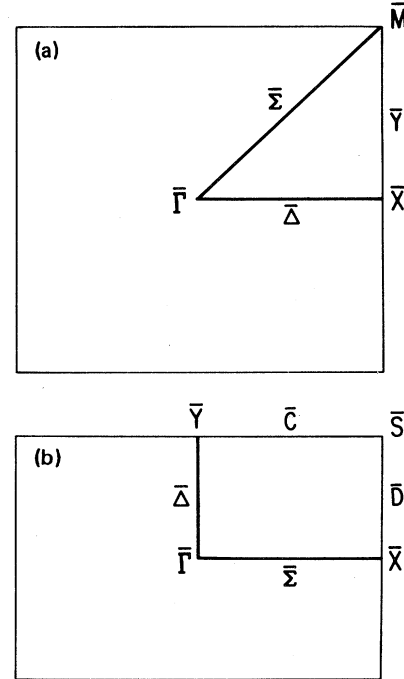


FIG. 1. Symmetry points and lines of the irreducible part of the two-dimensional BZ for (a) the Ni(100) surface and (b) the Ni(110) surface.

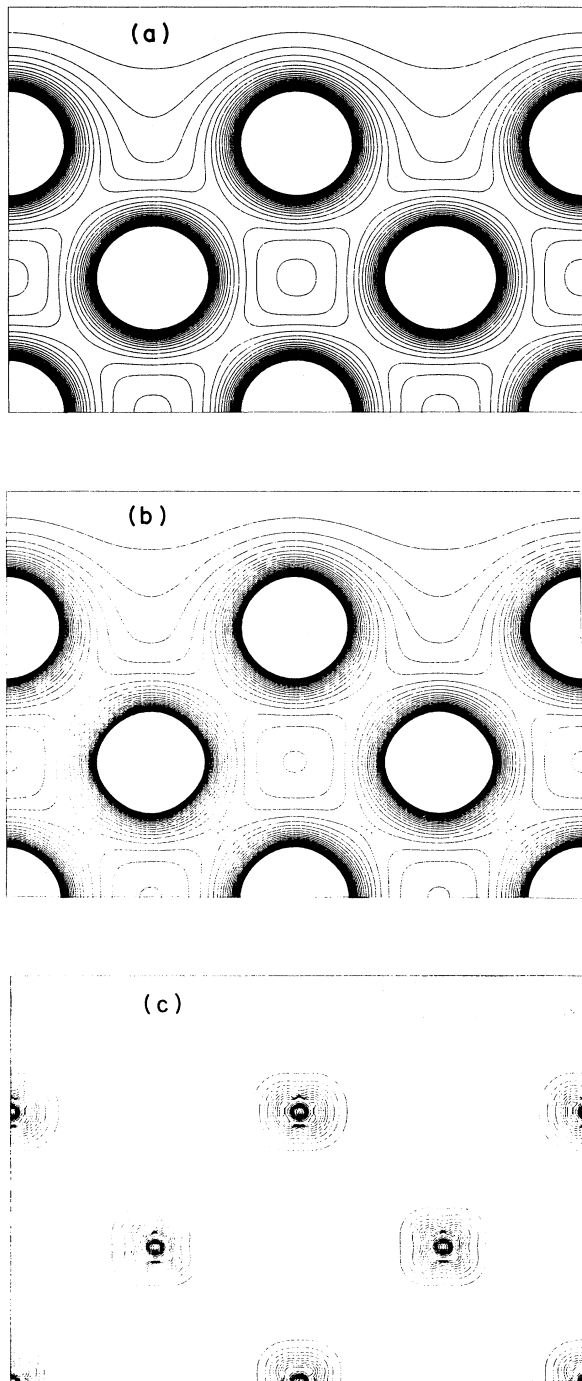


FIG. 2. Contour plot of (a) the majority-spin valence charge density for the Ni(100) five-layer slab, for a plane which is normal to the surface and passes through the face of the conventional bulk unit cell of the fcc Ni crystal. The smallest contour value is 0.3 (in units of electrons per bulk Ni unit cell—or  $0.004\,08\text{ a.u.}^{-3}$ ), and adjacent contours differ by 0.3. (b) Contour plot of the minority-spin valence charge density. (c) Contour plot of the valence-only spin density. The smallest contour value is 2.204 (in units of electrons per bulk Ni in unit cell—or  $0.03\text{ a.u.}^{-3}$ ), and adjacent contours differ by 2.204.

consistency process for the five-layer slabs. Twenty-five  $k$  points were used for the one- and three-layer slabs. We consider self-consistency achieved when the rms difference between input and output potential is less than 10 mRy. In the course of the self-consistent iterations, the valence charge density was obtained using a histogram-type summation. In the last iteration the layer-projected density of states (DOS) was obtained from the same  $\vec{k}$ -point sets, but using the linear analytic triangle method.<sup>48,49</sup>

### III. RESULTS AND DISCUSSION

In this section we present results of self-consistent spin-polarized calculations on one- and five-layer slabs for the Ni(100) surface, and on one-, three-, and five-layer slabs for the Ni(110) surface. Our interest and most of the detailed analysis will focus on the five-layer slabs, since these more nearly approximate the physical conditions near the real surface. Results from the one- and three-layer slabs will be used mainly to elucidate the origins of some important features of these surfaces.

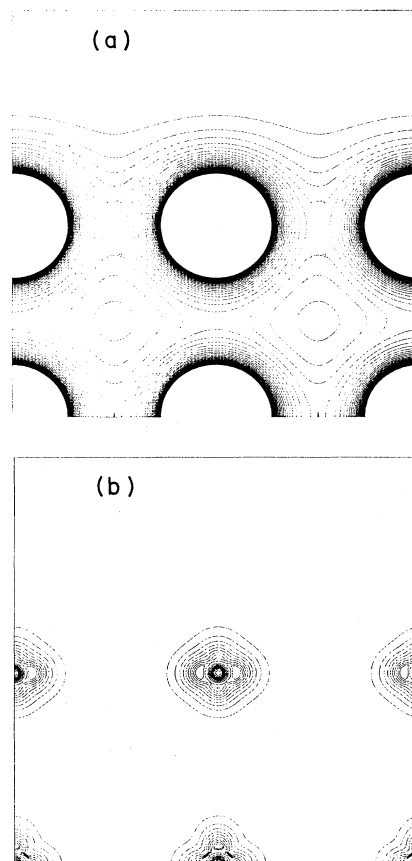


FIG. 3. Contour plot of the (a) majority-spin valence charge density for the Ni(110) five-layer slab, for a plane which is normal to the surface and which passes through the face of the conventional bulk unit cell of the fcc Ni crystal. Note that on the (110) surface this plane passes through the nucleus of the atoms in surface and central layers, but not through the nucleus of the subsurface layer atom. Contour values as in 2(a). (b) Contour plot of the valence-only spin density. Contour values as in 2(c).

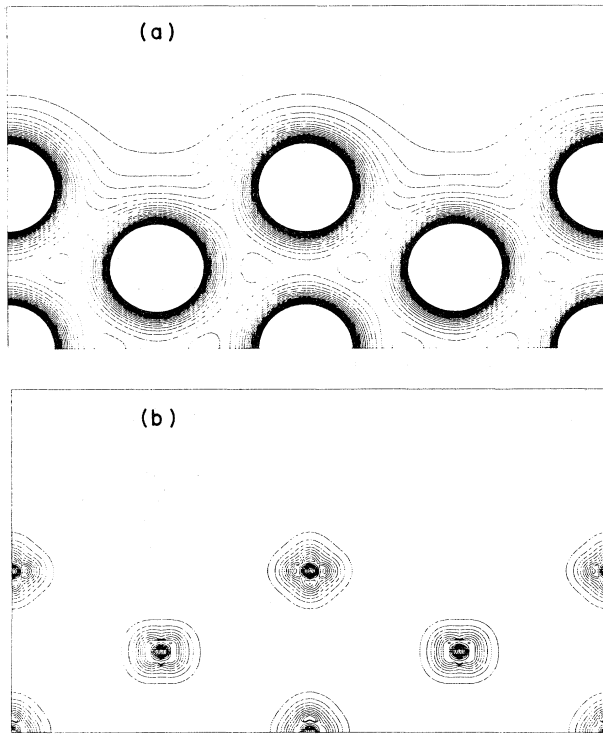


FIG. 4. Contour plot of (a) majority-spin valence charge density for the Ni(110) five-layer slab, for a plane which is normal to the surface and which passes through the nucleus of the atoms in surface, subsurface, and central layers (i.e., this vertical plane cuts the two-dimensional rectangular unit cell along the diagonal). Contour values as in 2(a). (b) Contour plot of the valence-only spin density. Contour values as in 2(c).

#### A. Charge density and spin density

We first examine our results for the majority- and minority-spin charge densities and their difference (the spin density), since these are of fundamental importance in local- (spin-) density-functional theory. Figure 2 presents the results for the Ni(100) five-layer slab, and Figs. 3 and 4 present the results for the Ni(110) five-layer slab. All of the contour plots in these figures are for vertical planes (i.e., normal to the surface), and only the upper half of the slab is shown since there is a mirror plane of  $z$ -reflection symmetry parallel to the surface and passing through the central layer of fcc (100) and (110) slabs (which have an odd number of layers). Because the majority- and minority-spin charge densities are very similar (Fig. 2), the minority-spin charge densities are not shown in Figs. 3 and 4. In preparing these contour plots, the spherical majority- and minority-spin core-electron densities were first subtracted, so only valence densities are depicted.

The most noticeable feature in these figures, as also found in other self-consistent calculations,<sup>48,49,51</sup> is the very rapid "healing" to bulklike character on going away from the surface and down into the interior of the solid. This is a consequence of the effective metallic screening of the surface perturbation. This screening is due to a sizable redistribution of charge in the surface layer, leading to the

formation of the "spill-out" dipole barrier which sensitively determines the work function.<sup>55</sup> For the Ni(100) surface, our work function for the five-layer slab is 5.5 eV. For the Ni(110) surface, our values are 5.2 and 5.1 eV for the three- and five-layer slabs, respectively. The experimental values are 5.22 eV for Ni(100) (Refs. 56 and 57) and 5.04 eV for Ni(110).<sup>56</sup> Jepsen *et al.*<sup>49</sup> reported a value of 5.4 eV, in good agreement with our result and with experiment. Self-consistency is, of course, crucial for obtaining an accurate value of the work function, and our results are in good agreement with the experimental values.

The form of the spill-out dipole barrier is quite complicated<sup>55</sup> since it has corrugations which follow the "hard-sphere" profile of the surface-vacuum interface. These corrugations are evident in the figures for the majority- and minority-spin charge densities. As pointed out by

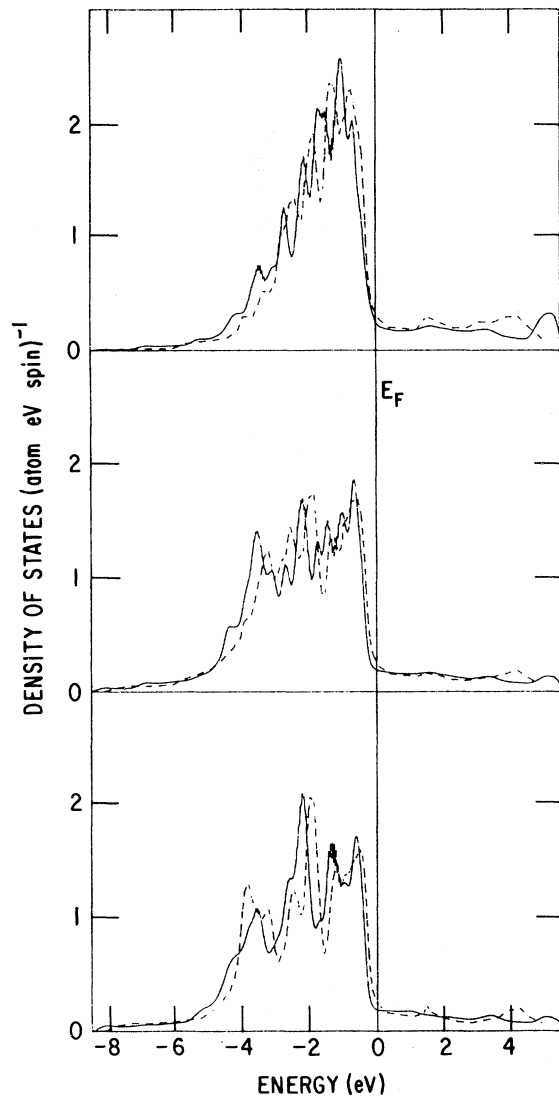


FIG. 5. Majority-spin layer-projected DOS for the five-layer Ni(100) slab (solid line) and for the five-layer Ni(110) slab (dashed line). The top, middle, and bottom panels are for the surface, subsurface, and central layers, respectively.

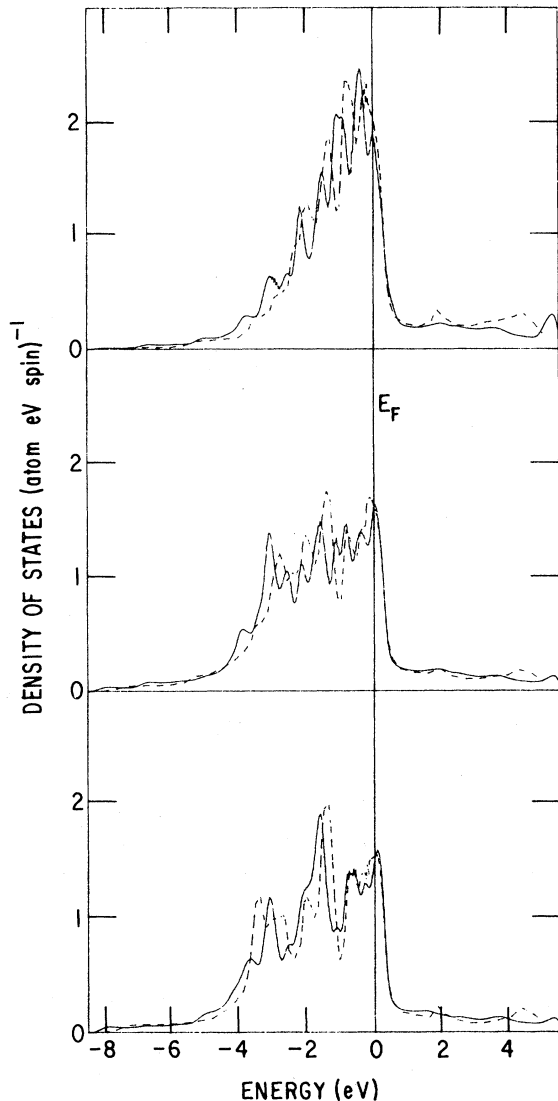


FIG. 6. Minority-spin layer-projected DOS for the five-layer Ni(100) slab (solid line) and for the five-layer Ni(110) slab (dashed line). The top, middle, and bottom panels are for the surface, subsurface, and central layers, respectively.

Hamann,<sup>58</sup> the only calculational techniques which can obtain highly accurate charge densities far into the vacuum region are those which use the Laue representation (parallel plane waves times numerical  $z$ -dependent functions) in this region—notably the pseudopotential scattering method and the LAPW method employed here. (Indeed, the limitations of the charge-density representation used in Ref. 48 are evident in Fig. 6 of Ref. 48, which displays an incorrect curvature for the corrugations far out in the vacuum. When our charge densities are plotted much further than shown in Figs. 2–4, the corrugations always have the same curvature which they have near the surface.) As expected, the steepest corrugations occur on the (110) surface for planes which cut the two-dimensional rectangular unit cell along the diagonal (Fig. 4). It is interesting to note the similarity between Fig. 2(a) for the

Ni(100) slab and Fig. 3 for the Ni(110) slab. For each slab, the contour plots in these figures are for a plane which passes through the cubic face of the conventional bulk unit cell of the fcc Ni crystal. Away from the surface, the densities are quite similar, as one can see by rotating the plane of Fig. 2 by  $45^\circ$  relative to that in Fig. 3.

Finally, it is worth noting that Hamann<sup>58</sup> has recently used such first-principles surface charge densities to construct He-atom–surface interaction potentials in order to analyze atomic-beam diffraction intensities from surfaces. Our spin-polarized results may be able to provide an improvement of this approach for ferromagnetic surfaces.

### B. Density of states

A good overview of the electronic and magnetic properties can be obtained from examination of the layer-projected DOS for the five-layer Ni slabs. The DOS for the majority- and minority-spin states are shown in Figs. 5 and 6, respectively. These curves have been Gaussian broadened (full width at half maximum of 0.2 eV) to suppress numerical noise; the solid line indicates the DOS for the Ni(100) slab and the dashed line indicates the DOS for the Ni(110) slab.

The DOS of the central atom in both five-layer slabs are seen to be nearly identical in shape. The upper  $d$ -band edges are within about 0.1 eV of each other (this is true also of the DOS for the other layers). Further below the Fermi energy the Ni(110) DOS seems narrowed compared to that of the Ni(100) slab, and major peaks are shifted nearer to  $E_F$  by about 0.2 eV. These differences in the central layer DOS, which should approximate the bulk DOS if the slab were thick enough, are largely size effects due to the finite thickness of the slabs. In the case of the Ni(110) slab, size effects are expected to be more pronounced, since the thickness of the (110) slab is reduced by a factor of  $\sqrt{2}$  from that of the (100) slab.

The DOS exhibits a marked narrowing in both slabs on going from the interior layers to the surface due to the reduced coordination number of the surface atom. [The coordination of surface and subsurface atoms for the fcc crystal is 8 and 12, respectively, for the (100) surface, and 7 and 11, respectively, for the (110) surface.] The exchange splitting in all layers is about 0.6 eV, as is found also in bulk Ni calculations.<sup>1,3,4</sup> That Ni is a *strong* ferromagnet is reflected in the fact that the majority-spin  $d$  band is fully occupied in all cases in Fig. 5. Significantly, this is true also at the surface, confirming the results of other theoretical calculations<sup>48,49</sup> that the Ni surface is not magnetically dead.

### C. Energy bands and surface states

In this section we discuss our results for the Ni(100) and Ni(110) five-layer slab energy-band structure and compare these to other calculations and experimental results.

#### 1. Ni(100) Energy bands and surface states

The majority-spin energy bands along the high-symmetry directions in the BZ are shown in Figs. 7 and 8, and the minority-spin bands are shown in Figs. 9 and 10. States of  $\bar{\Delta}_1\text{-}\bar{Y}_2\text{-}\bar{\Sigma}_1$  symmetry are shown separately (Figs. 7 and 9) from those of  $\bar{\Delta}_2\text{-}\bar{Y}_2\text{-}\bar{\Sigma}_2$  symmetry (Figs. 8 and 10).

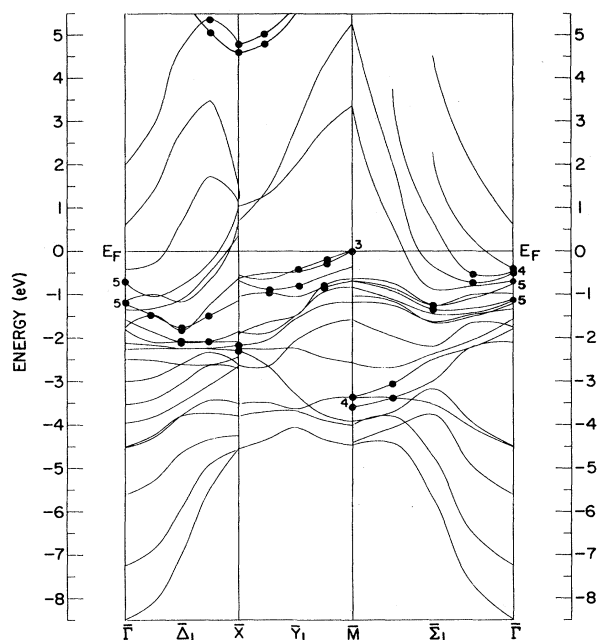


FIG. 7. Majority-spin energy bands of the five-layer Ni(100) slab, showing states of  $\bar{\Delta}_1\text{-}\bar{\Gamma}_1\text{-}\bar{\Sigma}_1$  symmetry. At the symmetry points, only states whose symmetry is compatible with these are shown. States which are localized in the surface layer are indicated by the closed circles. The small numbers label the two-dimensional irreducible representations at symmetry points in nonobvious cases.

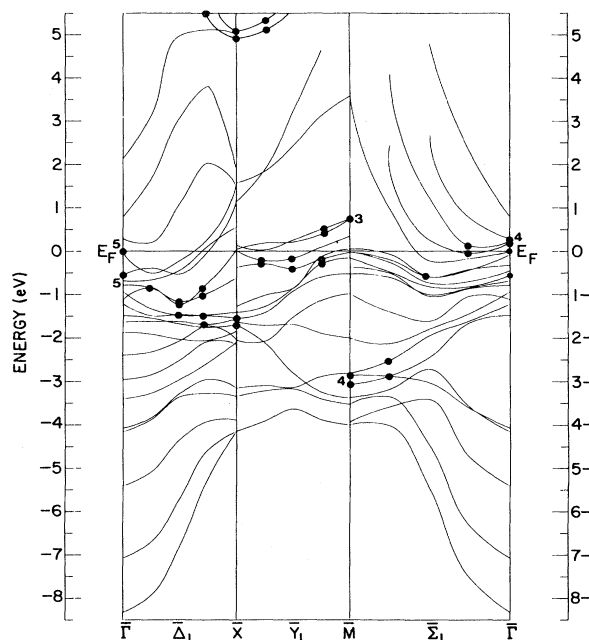


FIG. 9. Minority-spin energy bands of the five-layer Ni(100) slab, showing states of  $\bar{\Delta}_1\text{-}\bar{\Gamma}_1\text{-}\bar{\Sigma}_1$  symmetry.

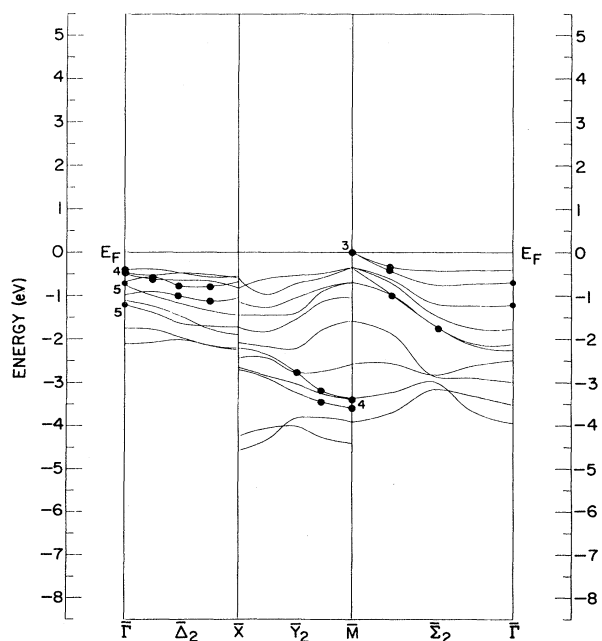


FIG. 8. Majority-spin energy bands of the five-layer Ni(100) slab, showing states of  $\bar{\Delta}_2\text{-}\bar{\Gamma}_2\text{-}\bar{\Sigma}_2$  symmetry.

The states of  $\bar{\Delta}_1\text{-}\bar{\Gamma}_1\text{-}\bar{\Sigma}_1$  symmetry are symmetric with respect to mirror-plane reflections corresponding to the given symmetry line, while the  $\bar{\Delta}_2\text{-}\bar{\Gamma}_2\text{-}\bar{\Sigma}_2$  states are antisymmetric with respect to the mirror-plane reflection. At the symmetry points, only states whose symmetry is compatible with these are shown. States which are localized in the surface layer are indicated by the closed circles. The small numbers label the two-dimensional irreducible representations of those localized states whose symmetry is not obviously determined by the compatibility relations at the symmetry points. The only bands which cross in these figures are bands of opposite  $z$ -reflection symmetry.

The most apparent feature of Figs. 7–10 is the similarity between the overall shape of the majority-spin bands and the minority-spin bands, the principal difference being the exchange splitting. Thus the occurrence of exchange-split surface states and resonances is the rule rather than the exception. In many cases, however, the minority-spin localized state is unoccupied while the majority-spin state is occupied. Only the occupied states are seen in photoemission experiments, of course, but new techniques such as inverse photoemission<sup>30</sup> may be used to experimentally verify the occurrence of surface states of both spins in these cases. In these figures, surface states are also seen to occur in pairs. This is a feature of the finite thickness of the slabs used to simulate the surface. The finite thickness slab actually has *two* surfaces, and surface states with decay lengths of a few layers can often overlap in thin slabs. In the limit of infinitely thick slabs, surface states localized on either surface would be degenerate. Thus the size of the splitting, in a given figure, between a pair of localized states reflects the degree of localization of the states at the surface. For example, the  $\bar{M}_3$  surface state in Figs.

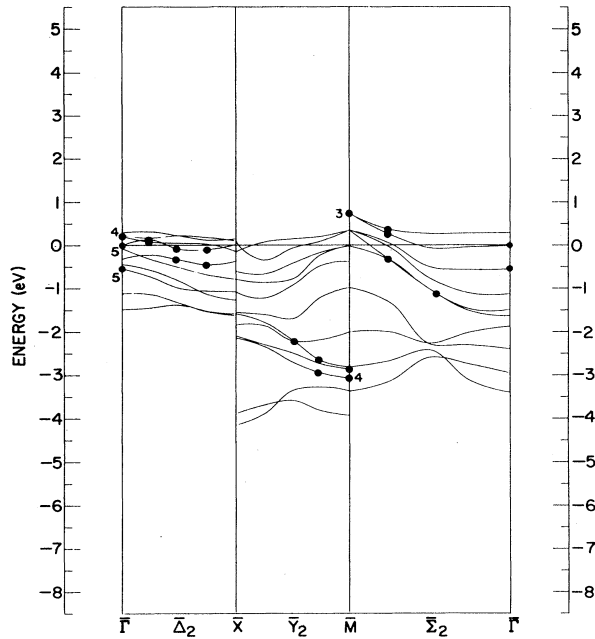


FIG. 10. Minority-spin energy bands of the five-layer Ni(100) slab, showing states of  $\bar{\Delta}_2$ - $\bar{Y}_2$ - $\bar{\Sigma}_2$  symmetry.

7 and 9 appears as a single closed circle near  $E_F$ , since this is a very localized state (about 95% in the surface layer) and the splitting is less than 1 mRy. By contrast, the  $\bar{\Gamma}_5$  surface state in Fig. 7 is much less localized (about 60% in the surface layer). Clearly, many of the above general remarks will also apply to the Ni(110) bands to be discussed below.

Starting with the highest-energy localized states, there is an unoccupied free-electron-like surface band centered at  $\bar{X}$ , about 5.0 eV above  $E_F$  in Figs. 7 and 9. The exchange splitting of this state is about 0.3 eV. As mentioned, there is a very localized  $\bar{M}_3$  surface state in Figs. 7–10. The majority state is within 1 mRy of  $E_F$ , while the minority-spin  $\bar{M}_3$  state is about 0.75 eV above  $E_F$ . This state disperses downward in energy becoming a  $\bar{Y}_1$  and  $\bar{\Sigma}_2$  resonance. Thus there is no majority-spin  $d$  hole at the  $\bar{M}$ -symmetry point as was found in Ref. 48. At  $\bar{\Gamma}$  there is a very localized (90% in the surface layer)  $\bar{\Gamma}_4$  surface state. The majority-spin state is about 0.5 eV below  $E_F$ , and the minority-spin state is about 0.25 eV above  $E_F$ . This state disperses downward along the  $\bar{\Delta}_2$ - and  $\bar{\Sigma}_1$ -symmetry lines as a surface resonance. Just below the  $\bar{\Gamma}_4$  state at  $\bar{\Gamma}$  there is a diffuse (about 60% localization in the surface layer)  $\bar{\Gamma}_5$  surface state. The majority-spin  $\bar{\Gamma}_5$  state is centered about 1.0 eV below  $E_F$ , and the minority-spin state is centered about 0.3 eV below  $E_F$ . Finally, there is a low-lying  $\bar{M}_4$  surface state: The majority-spin state is centered about 3.5 eV below  $E_F$ , and the minority-spin state is centered about 3.0 eV below  $E_F$ . The exchange splitting of  $d$ -band states is thus seen to decrease slightly on going down in energy away from  $E_F$ .

The bands and surface states in Figs. 7–10 are in good overall agreement with those of Wang and Freeman,<sup>78</sup> although there are some differences. As stated, we do not

find a majority-spin  $d$  hole at the  $\bar{M}$ -symmetry point, and the  $\bar{\Gamma}_5$  surface state was found to lie slightly higher than the  $\bar{\Gamma}_4$  surface state in the majority-spin bands. In Ref. 48 the majority-spin  $\bar{\Gamma}_5$  state was found 0.24 eV below  $E_F$  and the majority-spin  $\bar{\Gamma}_4$  state was found 0.33 eV below  $E_F$ . The surface localization of these states, however, is in good agreement with that obtained here. Some part of these differences (especially for the  $\bar{\Gamma}_5$  state which is more sensitive to the thickness of the slab) is due to the thicker slab (nine layers) used in Ref. 48. By contrast, Dempsey *et al.*<sup>38,39,59</sup> found a majority-spin  $\bar{\Gamma}_5$  surface state only 0.08 eV below  $E_F$ . They used the existence of this state to explain the sign change in the electron-spin-polarization measurements<sup>40–44</sup> 0.1 eV above threshold from Ni(100) and Ni(111). In agreement with Wang and Freeman, we find this state too far below  $E_F$  and too diffuse to support this mechanism.

Plummer and Eberhardt<sup>35</sup> have obtained angle-resolved photoelectron spectra for the Ni(100) surface, and have reported two bands of surface states. They found a  $\bar{\Sigma}_2$  band starting at the  $\bar{M}$ -symmetry point and going about halfway towards the  $\bar{\Gamma}$ -symmetry point. They also found a  $\bar{\Delta}_1$  band starting at the  $\bar{X}$ -symmetry point and going about a third of the way towards the  $\bar{\Gamma}$ -symmetry point. Both of these bands were located less than 0.1 eV below  $E_F$  and showed no dispersion. Significantly, they did not see the  $\bar{\Gamma}_5$  surface state in normal-exit photoemission (the  $\bar{\Gamma}_4$  state cannot be seen because of symmetry selection rules), which is consistent with the rather diffuse nature of this state. Erskine,<sup>37</sup> however, has reported the existence of a symmetry-allowed surface feature in his photoelectron spectra about 0.11 eV below  $E_F$ , and this would support the argument of Dempsey *et al.*<sup>38,39</sup> It should be noted,

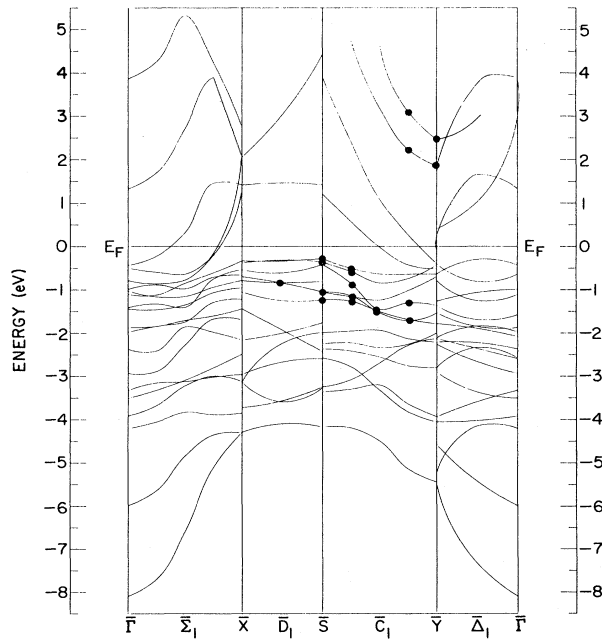


FIG. 11. Majority-spin energy bands of the five-layer Ni(110) slab, showing states of  $\bar{\Sigma}_1$ - $\bar{D}_1$ - $\bar{C}_1$ - $\bar{\Delta}_1$  symmetry.

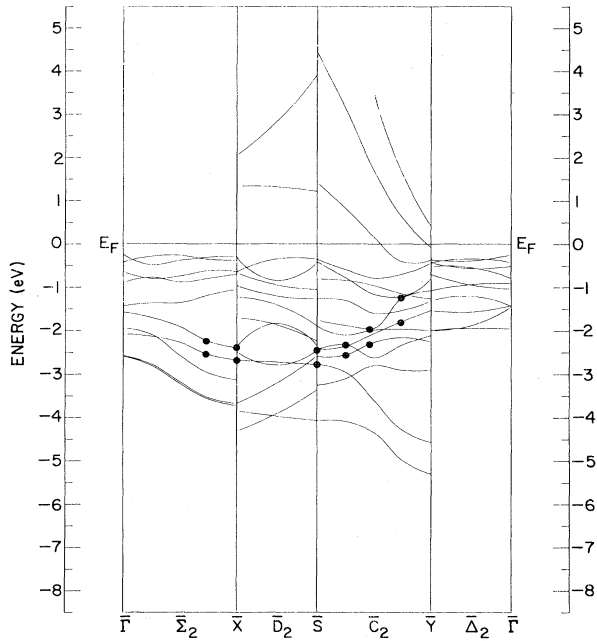


FIG. 12. Majority-spin energy bands of the five-layer Ni(110) slab, showing states of  $\bar{\Sigma}_2$ - $\bar{D}_2$ - $\bar{C}_2$ - $\bar{\Delta}_2$  symmetry.

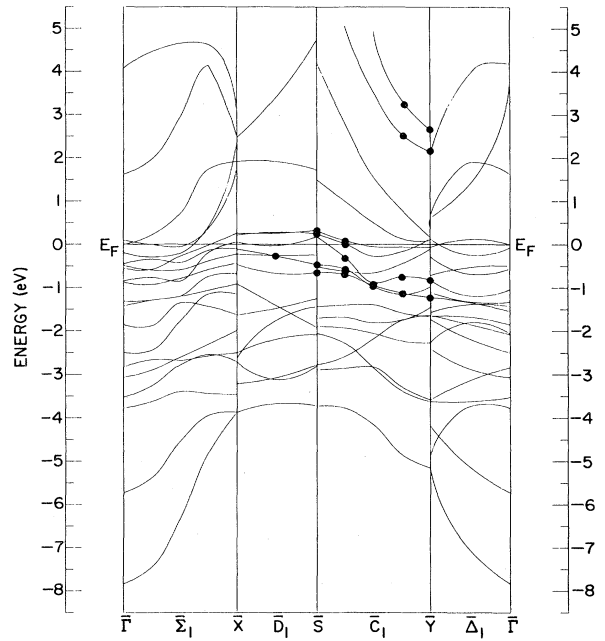


FIG. 13. Minority-spin energy bands of the five-layer Ni(110) slab, showing states of  $\bar{\Sigma}_1$ - $\bar{D}_1$ - $\bar{C}_1$ - $\bar{\Delta}_1$  symmetry.

however, that Plummer and Eberhardt<sup>35</sup> also reported a sharp feature in normal emission at the  $\bar{\Gamma}$ -symmetry point, but they specifically ruled it out as a surface state. Experimentally, Plummer and Eberhardt required that any possible surface-related feature in their spectra satisfy three tests or criteria for identifying a surface state: (1) It should be sensitive to surface contamination, (2) it should have no dispersion as the perpendicular component of the momentum is changed, and (3) the energy and parallel momentum of the structure should lie within a gap of the bulk band structure. The structure which they found at the  $\bar{\Gamma}$ -symmetry point in normal emission failed the second test. Using their third criterion, however, they assigned their  $\bar{\Delta}_1$  band to the minority-spin band and the  $\bar{\Sigma}_2$  band to the majority-spin band. The  $\bar{\Sigma}_2$  band is present in our calculation in Fig. 8, but our band has a fairly large dispersion downward. It is interesting to note that the experimental result for the  $\bar{\Sigma}_2$  band seems to confirm our finding of no  $d$ -band hole at the  $\bar{M}$ -symmetry point. Turning to the  $\bar{\Delta}_1$  minority-spin band of Plummer and Eberhardt, we do not find any such band in our calculation. Our  $\bar{\Delta}_1$  minority-spin band (Fig. 9) is about 1.0 eV below  $E_F$  at its highest point and drops to about 1.7 eV below  $E_F$  at the  $\bar{X}$ -symmetry point. On the other hand, our  $\bar{\Delta}_2$  minority-spin band is just below  $E_F$ .

## 2. Ni(110) energy bands and surface states

The majority-spin energy bands along the high-symmetry directions in the rectangular BZ of the Ni(110) five-layer slab are shown in Figs. 11 and 12, and the minority-spin bands are shown in Figs. 13 and 14. States of  $\bar{\Sigma}_1$ - $\bar{D}_1$ - $\bar{C}_1$ - $\bar{\Delta}_1$  symmetry are shown separately (Figs. 11 and 13) from those of  $\bar{\Sigma}_2$ - $\bar{D}_2$ - $\bar{C}_2$ - $\bar{\Delta}_2$  symmetry (Figs. 12

and 14). The occurrence of localized surface states is the same for the majority-spin and minority-spin bands. The minority-spin surface states are simply shifted to reduced binding energy by the exchange splitting.

There is a high-lying unoccupied free-electron-like  $\bar{C}_1$

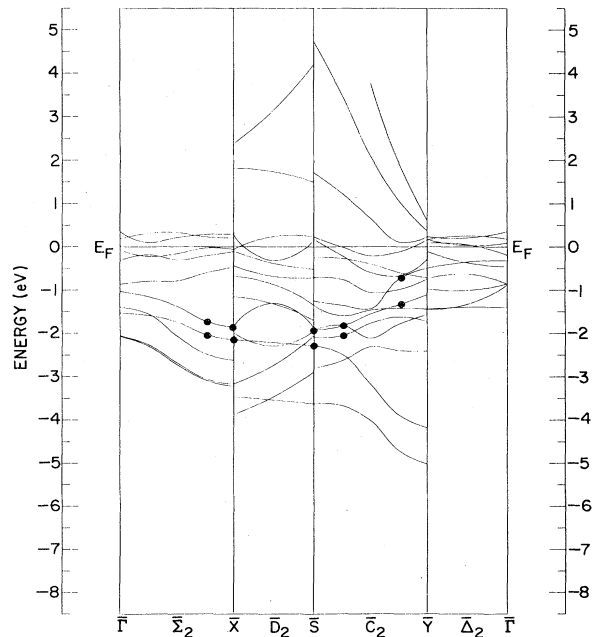


FIG. 14. Minority-spin energy bands of the five-layer Ni(110) slab, showing states of  $\bar{\Sigma}_2$ - $\bar{D}_2$ - $\bar{C}_2$ - $\bar{\Delta}_2$  symmetry.

band between 2.0 and 3.0 eV above  $E_F$  in Figs. 11 and 13. As might be guessed from the splitting between  $z$ -reflection pairs, this state has only about 55–60% localization in the two surface layers. At the  $\bar{S}$ -symmetry point (the corner of the rectangular BZ) there is a very localized  $\bar{S}_1$  surface state (about 85% in the surface layer). The majority-spin  $\bar{S}_1$  state is about 0.3–0.4 eV below  $E_F$ , and the minority-spin state is about 0.2–0.3 eV above  $E_F$ . This state disperses downward in energy along the  $\bar{C}_1$ -symmetry line. At about 1.0–2.0 eV below  $E_F$  in Fig. 11 and 0.5–1.5 eV below  $E_F$  in Fig. 13, there is another surface-resonance band of  $\bar{D}_1$ - $\bar{S}_1$ - $\bar{C}_1$ - $\bar{Y}_1$  symmetry. Finally, there is a low-lying  $\bar{S}_2$  and  $\bar{C}_2$  surface-resonance band 1–3 eV below  $E_F$  in Figs. 12 and 14.

The most highly localized of these states is the exchange-split  $\bar{S}_1$  surface state near  $E_F$ . In a non-self-consistent Ni(110) slab calculation, Dempsey *et al.*<sup>59</sup> found two  $\bar{S}_2$  and  $\bar{S}_1$  minority-spin surface states and only a single  $\bar{S}_2$  majority-spin surface state. The degree of localization of these states was not reported in Ref. 59. Keeping in mind the fact that  $d$ -band surface states can be very sensitive to the surface potential, it is possible that the  $\bar{S}_2$  surface state in Ref. 59 is the same as the  $\bar{S}_1$  surface state reported here (the  $\bar{S}_1$  vs  $\bar{S}_2$  symmetry depends on whether the surface atomic plane has its atom at the unit-cell center or at the corner<sup>59</sup>).

The observation of an exchange-split Ni(110) SS near  $E_F$  at  $\bar{S}$  was studied by Eberhardt *et al.*<sup>36</sup> using angle-resolved photoemission spectroscopy. The symmetry of these states was incorrectly assigned in Ref. 36, however, as pointed out by Kleinman.<sup>60</sup> The completely symmetric  $S_1$  symmetry of the states found in our calculation is, therefore, consistent with the observations of Eberhardt *et al.*<sup>36</sup> Experimentally, these states were assigned to the majority-spin and minority-spin bands on the basis of comparison with bulk band structure. Further experimental evidence of their magnetic character was the observed temperature dependence of their splitting. At low temperatures (100 K), the experimental exchange splitting is 0.3 eV in agreement with the observed splitting of the bulk Ni bands.<sup>26</sup> While the calculated position of the majority-spin state in Fig. 11 is 0.32 eV below  $E_F$  and in good agreement with experiment, the minority-spin state in Fig. 13 is unoccupied and 0.30 eV above  $E_F$ . This yields a theoretical exchange splitting of 0.62 eV, about twice as large as the experimental result. Interestingly, this is also the same discrepancy in the bulk exchange splitting between theory<sup>3</sup> and experiment.<sup>26</sup> As mentioned, it seems to be now generally accepted that this discrepancy in bulk exchange splitting can be accounted

TABLE I. Ni(100) slabs—orbital decomposition [ $l=0,1,2$  ( $s,p,d$ )] of the total number of electrons (i.e., both spins) in the muffin-tin spheres, where  $S$ ,  $S-1$ , and  $C$  denote the surface, subsurface, and center atoms, respectively.

Slab	Layer	$s$	$p$	$d$
One layer		0.42	0.15	8.26
Five layer	$S$	0.43	0.29	8.29
	$S-1$	0.46	0.42	8.29
	$C$	0.46	0.43	8.28

TABLE II. Ni(110) slabs—orbital decomposition [ $l=0,1,2$  ( $s,p,d$ )] of the total number of electrons (i.e., both spins) in the muffin-tin spheres, where  $S$ ,  $S-1$ , and  $C$  denote the surface, subsurface, and center atoms, respectively.

Slab	Layer	$s$	$p$	$d$
One layer		0.38	0.07	8.29
Three layer	$S$	0.42	0.25	8.31
	$C$	0.45	0.37	8.27
Five layer	$S$	0.42	0.24	8.30
	$S-1$	0.45	0.39	8.29
	$C$	0.46	0.41	8.30

for by unequal values of the many-body self-energy shifts for the majority-spin versus the minority-spin bands.<sup>14–23</sup>

Thus small energy shifts of about 0.3 eV could easily bring our calculated  $S_1$  bands into exact agreement with the observations of Eberhardt *et al.* Our theoretical determination of highly localized (85%) surface states at  $S_1$  represents strong theoretical evidence that magnetically split surface states were indeed observed by Eberhardt *et al.*, i.e., that their measurements are truly determined by the surface electronic structure and not by the underlying bulk bands. The good agreement between our calculation and the measurements of Eberhardt *et al.* further confirms the absence of magnetically dead layers on the Ni surface.

#### D. Enhanced surface magnetization

Since the magnetization is essentially zero (less than about  $\pm 0.1\mu_B$ ), outside the muffin-tin spheres, we focus our attention on the charge and spin density inside these spheres and present in Tables I and II detailed information about the orbital decomposition of the total charge. The magnetic moment inside the sphere is essentially that of the  $d$  electrons (again to within about  $0.1\mu_B$ ), and Tables III and IV present the majority- and minority-spin  $d$ -charge and  $d$ -magnetic moments inside the muffin-tin spheres. All the numbers in Tables I–IV were obtained by integrating the  $l$ -decomposed majority-spin and/or minority-spin density inside the spheres. It should be remembered that these densities were obtained by using a histogram-type method for performing the BZ integrations, as described in Sec. II. This is also the way in which the densities were obtained in the course of the self-consistent iterations. A more accurate method for performing BZ sums (especially for metals) is the linear analytic triangle method.<sup>48,49</sup> Using the final self-consistent energies and wave functions for the five-layer slabs, this method was also used to “analytically” integrate the layer-projected DOS of Figs. 5 and 6. The magnetic moments obtained in this manner are given in parentheses in Tables III and IV. In all cases, the magnetic moment at the surface is *larger* than that of the interior atoms. The effect of using the linear triangle method is simply to reduce the magnitude of the moment in each layer, while preserving the trend. Even for the three-layer Ni(110) slab, the moment is larger at the surface by the same amount as in the five-layer Ni(110) slab. The magnetic moment for the Ni(100) and Ni(110) monolayers is  $0.86\mu_B$  and  $0.96\mu_B$ , respectively. These values are much larger

TABLE III. Ni(100) slabs— $d$ -electron contribution to the magnetic moment (in  $\mu_B$ ) in the muffin-tin spheres. For the five-layer slab, the magnetic moment calculated using the linear-analytic triangle method is shown in parentheses.  $S$ ,  $S-1$ , and  $C$ , denote the surface, subsurface, and center atoms, respectively.

Slab	Layer	$d$ -Maj	$d$ -Min	$d$ -Tot	Moment
One layer		4.56	3.70	8.26	0.86
Five layer	$S$	4.51	3.78	8.29	0.73 (0.64)
	$S-1$	4.48	3.80	8.29	0.68 (0.55)
	$C$	4.49	3.80	8.28	0.69 (0.54)

than any of the moments in the thicker films. Noffke and Fritsche<sup>61</sup> also obtained a large value for the  $d$  moment ( $0.88\mu_B$ ) for the Ni(100) monolayer.

In the first spin-polarized self-consistent calculation on any surface, Wang and Freeman<sup>48</sup> found a strong Friedel oscillation in the spin density for a nine-layer Ni(100) slab. By contrast, we find that the central and subsurface atoms of the five-layer Ni(100) slab have essentially the same magnetic moments and the same  $s$ ,  $p$ , and  $d$  charge. This seems to rule out any significant Friedel oscillations of the charge or spin density.<sup>48</sup> Furthermore, another important feature to emerge in Tables I and II is that the total  $d$  charge of the surface atom is virtually identical to that of the interior atoms. These results are in general agreement with those of Jepsen *et al.*<sup>49</sup> but disagree with those of Wang and Freeman.<sup>48</sup> The same features are true for the Ni(110) slab. Thus Jepsen *et al.*<sup>49</sup> found magnetic moments of  $0.61\mu_B$ ,  $0.55\mu_B$ , and  $0.58\mu_B$  for the surface, subsurface, and central atoms, respectively, for a Ni(100) five-layer slab, using the linear-triangle method. Their results are in rather good agreement, not only in the trend, but also in magnitude with the values in parentheses in Table III. By contrast, a *reduced* surface moment was found in Ref. 48 for their nine-layer Ni(100) calculation. As noted above, however, there is generally good agreement for spectral features such as DOS and surface states between Ref. 48 and the results of the present calculation. The magnetization density is a small quantity (the difference between two larger densities), and the basis set limitations combined with restrictions in the representation of the charge density in the pioneering LCAO calculation of Ref. 48 probably are responsible for this discrepancy.

Comparing the results of Jepsen *et al.* with our results in Table III, and comparing our three-layer results with our five-layer results in Table IV, suggests the following conclusions. While differences in size effects and  $k$ -point

sampling (i.e., the number of  $k$  points at which energies and wave functions are calculated—and the method by which BZ integrations are performed) between various calculations may yield somewhat different numerical results, two trends are expected in any *one* accurate self-consistent calculation. It is argued below that these trends can be expected in all other three-dimensional ferromagnetic transition-metal surfaces as well.

(1) *Layer-by-layer charge neutrality.* The  $s$ ,  $p$ , and  $d$  charge of the interior atoms (e.g.,  $S-1$  and  $C$  in Tables I and II) will be virtually identical. Furthermore, the *total*  $d$  charge of the surface atom will be essentially the same as for the interior atoms, and the “missing”  $s$  and  $p$  charge in the surface atom is accounted for by the spill-out charge into the vacuum. Thus each layer is charge neutral.

(2) *Enhanced surface moment.* The magnetic moment of the surface atom will be larger than that of the interior atoms, while the interior atoms will all have nearly identical moments (reflecting the efficiency of the metallic screening of the surface). As discussed below, this enhancement is due to two additive mechanisms: (i) the presence of electrostatic shifts which are necessary to maintain the layer-wise charge neutrality, and (ii) the relative dehybridization of  $sp$ - and  $d$ -electron states at the surface atom compared to an interior atom.

We have confidence in the conclusion stated in (1) above for the following reasons. The localized character of the  $d$  orbitals and the requirement of layer-wise charge neutrality (substantiated in many other self-consistent calculations for  $d$ -band metals) effectively constrains the total number of  $d$  electrons inside the muffin-tin spheres of each layer to be equal. Jepsen *et al.*<sup>49</sup> find this value to be 8.34 electrons in their Ni(100) five-layer slab, while we find  $8.29 \pm 0.01$  electrons (Tables I and II). While these values differ by 0.05 electrons, it should be noted that they used touching muffin-tin spheres, whereas we used spheres of

TABLE IV. Ni(110) slabs— $d$ -electron contribution to the magnetic moment (in  $\mu_B$ ) in the muffin-tin spheres. For the five-layer slab, the magnetic moment calculated using the linear-analytic triangle method is shown in parentheses.  $S$ ,  $S-1$ , and  $C$  denote the surface, subsurface, and center atoms, respectively.

Slab	Layer	$d$ -Maj	$d$ -Min	$d$ -Tot	Moment
One layer		4.63	3.67	8.29	0.96
Three layer	$S$	4.54	3.77	8.31	0.77
	$C$	4.48	3.79	8.27	0.69
Five layer	$S$	4.50	3.80	8.30	0.70 (0.63)
	$S-1$	4.45	3.83	8.29	0.62 (0.54)
	$C$	4.46	3.84	8.30	0.62 (0.56)

TABLE V.  $3p_{3/2}$  core-level energies of the three- and five-layer Ni(110) slabs and of the five-layer Ni(100) slab. Note that the splitting due to spin-polarization in any layer is larger than the splitting between the central and surface layers of a given spin. Energies are relative to the Fermi energy (in eV).  $S$ ,  $S-1$ , and  $C$  denote the surface, subsurface, and center atoms, respectively.

Slab	Layer	Maj	Min	Min - Maj
Ni(110), three layer	$S$	-62.53	-61.71	0.82
	$C$	-62.83	-62.09	0.74
	$S-C$	0.30	0.38	
Ni(110), five layer	$S$	-62.38	-61.76	0.62
	$S-1$	-62.73	-62.13	0.60
	$C$	-62.82	-62.22	0.60
	$S-C$	0.44	0.46	
Ni(100), five layer	$S$	-62.54	-61.80	0.74
	$S-1$	-62.89	-62.18	0.71
	$C$	-62.92	-62.20	0.72
	$S-C$	0.38	0.40	

about 1.5% smaller radius. (The reasons for this choice are unimportant. Touching spheres could have been used. The correct bulk Ni lattice spacing was, of course, employed with  $a=6.65$  a.u.) This fact, taken together with the different  $k$ -point sampling, accounts for the difference. The important point, however, is that the requirement of charge neutrality yields the same value of the total  $d$  charge in each layer for any given accurate self-consistent calculation. In fact, if the charge density in each layer and in the vacuum as not converged to a high degree of accuracy, the calculated work functions would differ greatly from the experimentally measured work functions (theoretical and experimental work-function values are given in Sec. III A). The good agreement between our work-function value and that of Jepsen *et al.*<sup>49</sup> with the experimental value demonstrates that both LAPW calculations have correctly treated the various charge transfers which occur near the surface. We have confidence, therefore, in the important result that the total number of  $d$  electrons is the same in every atom of the clean Ni surface.

We now turn to the conclusions in (2) above. Regarding the mechanism of electrostatic shifts, our basic argument is based on a model of surface core-level shifts (i.e., shifts relative to the same core level of an interior atom). A simple model of core-level shifts<sup>62</sup> assumes surface  $d$ -band narrowing (Figs. 5 and 6) and the same number of  $d$  electrons in atoms of each layer (which, as we have seen is confirmed by our calculation). This model predicts that if  $E_F$  falls above (below) the center of the  $d$  band, a shift to reduced (greater) binding energy will be observed. Non-self-consistent tight-binding calculations<sup>63,64</sup> for this model predict a sign change near the middle of the 5d transition series between Ta and W, and the shift on Ta(111) is indeed observed to be greater by 0.3 eV.<sup>65</sup> Similarly, a shift to reduced binding energy has been reported for the W(111) (Ref. 65) and W(110) (Ref. 66) surfaces. Self-consistent calculations for Ti,<sup>67</sup> Sc,<sup>68</sup> and Cu (Refs. 45, 69, and 70) also give shifts in agreement with this model. Shifts to reduced binding energy are also found here for both Ni(100) and Ni(110) (Table V). As mentioned, core-level shifts in the present calculation are in the direction of reduced binding energy and are also in

agreement with this simple model. In order to maintain a constant number of  $d$  electrons in the narrowed surface-layer DOS of the Ni surface, an electrostatic potential (presumably due to small charge rearrangements of the more itinerant  $s$  and  $p$  electrons) must shift the surface-layer DOS to reduced binding energy. This same electrostatic potential also shifts the surface core electrons to reduced binding energy relative to the interior atoms, thus explaining the observed core-level shifts.

The new feature in ferromagnetic metals is the presence of two  $d$ -band DOS in each layer, one for the majority-spin and one for the minority-spin states. The scenario is as follows: First the narrowing of both majority- and minority-spin  $d$  bands increases the total number of electrons of each spin in the surface layer. In order to maintain charge neutrality, both DOS curves must now be imagined to move to reduced binding energy (both by the same shift in energy—assuming the shape of the DOS for the spin-up and spin-down electrons is the same), and this now acts to decrease the total number of electrons of each spin. The crucial point is that  $E_F$  falls near a peak of the minority-spin DOS (this makes the argument more specific to Ni). By contrast,  $E_F$  cuts the majority DOS in a region where it is relatively flat, since the majority  $d$  band is full (strictly speaking, nearly full, since  $s$ - $d$  hybridization results in some holes). Thus, for a given upward shift  $\Delta E$ , more electrons are removed from the minority-spin band than from the majority-spin band. Thus the majority-spin  $d$  band can actually gain some  $d$  electrons after this imagined two-step process is completed. This is, in fact, the case as shown in Tables III and IV. On the basis of this mechanism alone, we would predict that the surfaces of all ferromagnetic metals should have enhanced moments, since all three-dimensional metals have more than half-filled  $d$  bands. If there existed a ferromagnetic metal with a less than half-filled  $d$  band, this mechanism would predict a reduction in the surface moment relative to an interior atom. Support for this mechanism also comes from the fact that the increase of the surface moment over an interior atom moment is larger on the more open Ni(110) surface than on the Ni(100) surface (Tables III and IV). This in turn is consistent with the fact that the core-level shifts on the Ni(110) surface (0.45 eV) are

slightly larger than those on the Ni(100) surface (0.38 eV). Table V presents the chemical shifts of the surface  $3p_{3/2}$  core levels of the Ni(100) and Ni(110) slabs. Surface shifts for the other core levels are nearly the same. Note that the splitting due to spin polarization is larger than the chemical shift in all cases.

A second mechanism which also acts to increase the magnetic moment at the surface is the dehybridization of the  $s$ -,  $p$ -, and  $d$ -electron states at the surface, which like the electrostatic shift mechanism, is also ultimately related to the reduced coordination of the surface atom and the resulting narrowing of the  $d$  band. A striking measure of the effect of the lower coordination at the surface is the reduced  $l=1$  or  $p$ -state character of the muffin-tin charge (Tables I and II). In the case of the Ni(100) and Ni(110) monolayers, this loss of  $p$ -state character and large enhancement of magnetic moment is related to the lower coordination [four nearest neighbors on the Ni(100) monolayer and only two nearest neighbors for the Ni(110) monolayer] and the well-known<sup>50</sup> narrowing of the monolayer DOS. In the limit of the free atom, the  $4p$  states are, of course, unoccupied, and the magnetic moment reaches a maximum of  $2\mu_B$ . The  $p$  character in a given muffin-tin sphere is, in large part, due to the overlapping "tails" of  $s$ -like charge from neighboring atoms. The narrowing and consequent dehybridization is not as extreme for the surface Ni atom of the thicker slabs, but the same effect is present.

The phenomena of  $s$ - $d$  dehybridization and the results presented in Tables I–IV are also relevant to the issue of  $sp$ -to- $d$  charge transfer at transition-metal surfaces raised in Ref. 71. The results in Tables I–IV clearly support Kleinman's<sup>72</sup> critique of the Cu and Ni surface calculations of Tersoff and Falicov.<sup>71</sup> Our results support the conclusions of Ref. 72 that the  $d$ -electron charge is nearly identical in each layer. There is no evidence in our calculations for the phenomena of  $sp$ -to- $d$  charge transfer discussed in Ref. 71.

#### IV. CONCLUSION

We have presented results of detailed all-electron self-consistent semirelativistic local-spin-density investigations of the magnetism of several Ni( $hkl$ ) surfaces. Self-consistent LSDF calculations on the Ni(110) surface were reported for the first time for one-, three-, and five-layer slabs. In addition, parallel calculations for Ni(100) one-, and five-layer slabs were also reported. No magnetically dead layers were found. Instead, we predict a 13% enhancement compared to bulk of the Ni(110) surface magnetic moment, and a 7% enhancement for the Ni(100) surface moment. For Ni(100), our results are in good agreement with those of Jepsen *et al.*,<sup>49</sup> but disagree with the earlier work of Wang and Freeman<sup>48</sup> who found a

20% decrease in the surface moment. The enhanced moments on both surfaces are attributed to two additive effects:  $sp$ - $d$  dehybridization at the surface and the presence of electrostatic shifts required to maintain layer-by-layer charge neutrality. The total  $d$  electronic charge is the same in each layer, which contradicts the claim by Tersoff and Falicov<sup>71</sup> of  $sp$ -to- $d$  charge transfer at the surface of transition metals.

On the Ni(110) surface, an exchange-split highly localized surface state at the corner of the two-dimensional BZ is found which is in good agreement with the angle-resolved photoemission data of Eberhardt *et al.*<sup>36</sup> As in the case of bulk Ni, the theoretical exchange splitting 0.6 eV, is twice as large as that found experimentally and is attributed to neglected many-body effects.

On the Ni(100) surface it is found that surface states at the zone center are unable to account for the reversal above threshold of the spin polarization of photoemitted electrons. On the other hand, Moore and Pendry<sup>44</sup> calculated the photoelectron spin polarization of Ni(100) without surface states but using a smaller exchange splitting (about 0.3 eV), and obtained good agreement with experiment.

A majority-spin  $\bar{\Sigma}_2$  surface-resonance state on Ni(100) is in good agreement with the experimental surface state of Plummer and Eberhardt,<sup>35</sup> but has greater dispersion downward away from the Fermi energy than is found experimentally. We do not find the  $\bar{\Delta}_1$  minority-spin band observed by Plummer and Eberhardt just below the Fermi energy; instead we find a flat  $\bar{\Delta}_2$  minority-spin band about 0.5 eV below the Fermi energy.

Finally, we have found surface core-level shifts to reduced binding energy of 0.39 eV on Ni(100) and 0.4 eV on Ni(110). In the present calculation, the polarization of the core states by the valence electrons splits the majority- and minority-spin core states in each layer by about 0.6 eV (the theoretical exchange splitting). Since the surface core-level chemical shift found here is the same for each spin and smaller than the exchange splitting of the LSDF one-particle core states, it would be interesting if such separated manifolds could be observed experimentally. Each such manifold would be due to photoelectrons of the same spin polarization and would consist of two peaks split by the surface core-level shift.

#### ACKNOWLEDGMENTS

Research at The College of William and Mary was supported by the National Science Foundation (Grant No. DMR-81-20550). Research at Northwestern University and Argonne National Laboratory was supported by the National Science Foundation (Grant No. DMR-77-23776) and by the U.S. Department of Energy.

\*Permanent address: Institut für Physikalische Chemie, Universität Wien, Währingerstrasse 42, A-1090 Vienna, Austria.

<sup>1</sup>V. L. Moruzzi, J. F. Janak, and A. R. Williams, *Calculated Electronic Properties of Metals* (Pergamon, New York, 1978), and references therein.

<sup>2</sup>J. W. D. Connolly, *Phys. Rev.* **159**, 415 (1967).

<sup>3</sup>C. S. Wang and J. Callaway, *Phys. Rev. B* **15**, 298 (1977), and references therein.

<sup>4</sup>J. R. Anderson, D. A. Papaconstantopoulos, L. L. Boyer, and J. E. Schirber, *Phys. Rev. B* **20**, 3172 (1979).

<sup>5</sup>P. Hohenberg and W. Kohn, *Phys. Rev.* **136**, B864 (1964); W. Kohn and L. J. Sham, *Phys. Rev.* **140**, A1133 (1965).

<sup>6</sup>U. von Barth and L. Hedin, *J. Phys. C* **5**, 1629 (1972).

<sup>7</sup>O. Gunnarsson, B. I. Lundqvist, and S. Lundqvist, *Solid State Commun.* **11**, 149 (1972).

<sup>8</sup>A. K. Rajagopal and J. Callaway, *Phys. Rev. B* **7**, 1912 (1973).

<sup>9</sup>D. M. Edwards, *J. Magn. Magn. Mater.* **15–18**, 262 (1980).

- <sup>10</sup>R. E. Prange and V. Korenman, *Phys. Rev. B* **19**, 4691 (1979), and references therein.
- <sup>11</sup>J. Hubbard, *Phys. Rev. B* **19**, 2626 (1979).
- <sup>12</sup>H. Hasegawa, *J. Phys. Soc. Jpn.* **46**, 1504 (1979).
- <sup>13</sup>V. Korenman and R. E. Prange, *Phys. Rev. Lett.* **44**, 1291 (1980).
- <sup>14</sup>D. R. Penn, *Phys. Rev. Lett.* **42**, 921 (1979).
- <sup>15</sup>L. A. Feldkamp and L. C. Davis, *Phys. Rev. Lett.* **43**, 151 (1979).
- <sup>16</sup>L. C. Davis and L. A. Feldkamp, *J. Appl. Phys.* **50**, 1944 (1979).
- <sup>17</sup>A. Liebsch, *Phys. Rev. Lett.* **43**, 1431 (1979).
- <sup>18</sup>L. Kleinman, *Phys. Rev. B* **19**, 1295 (1979).
- <sup>19</sup>G. Treglia, F. Ducastelle, and D. Spanjaard, *Phys. Rev. B* **21**, 3729 (1980).
- <sup>20</sup>G. Treglia, F. Ducastelle, and D. Spanjaard, *Phys. Rev. B* **22**, 6472 (1980).
- <sup>21</sup>G. Treglia, F. Ducastelle, and D. Spanjaard, *J. Phys. (Paris)* **41**, 281 (1980).
- <sup>22</sup>A. Liebsch, *Phys. Rev. B* **23**, 5203 (1981).
- <sup>23</sup>L. Kleinman and K. Mednick, *Phys. Rev. B* **24**, 6880 (1981).
- <sup>24</sup>D. E. Eastman, F. J. Himpsel, and J. A. Knapp, *Phys. Rev. Lett.* **44**, 95 (1980).
- <sup>25</sup>D. E. Eastman, F. J. Himpsel, and J. A. Knapp, *Phys. Rev. Lett.* **40**, 1514 (1978).
- <sup>26</sup>F. J. Himpsel, J. A. Knapp, and D. E. Eastman, *Phys. Rev. B* **19**, 2919 (1979).
- <sup>27</sup>W. Eberhardt and E. W. Plummer, *Phys. Rev. B* **21**, 3245 (1980).
- <sup>28</sup>C. Rau, *Comments Solid State Phys.* **9**, 177 (1980).
- <sup>29</sup>R. J. Celotta, D. T. Pierce, G. C. Wang, S. D. Bader, and G. P. Felcher, *Phys. Rev. Lett.* **43**, 728 (1979). Also see R. Feder, *J. Phys. C* **14**, 2049 (1981), and references therein.
- <sup>30</sup>F. Himpsel and Th. Fausten, *Phys. Rev. B* **26**, 2679 (1982); D. P. Woodruff, N. V. Smith, P. D. Johnson, and W. A. Roger, *ibid.* **26**, 2943 (1982).
- <sup>31</sup>L. N. Leibermann, J. Clinton, D. M. Edwards, and J. Mathon, *Phys. Rev. Lett.* **25**, 232 (1970).
- <sup>32</sup>D. T. Pierce and H. C. Siegmann, *Phys. Rev. B* **9**, 4035 (1974).
- <sup>33</sup>G. Bergmann, *Phys. Rev. Lett.* **41**, 264 (1978).
- <sup>34</sup>R. Meservey, P. M. Tedrow, and V. R. Kalvey, *Solid State Commun.* **36**, 969 (1980).
- <sup>35</sup>E. W. Plummer and W. Eberhardt, *Phys. Rev. B* **20**, 1444 (1979).
- <sup>36</sup>W. Eberhardt, E. W. Plummer, K. Horn, and J. Erskine, *Phys. Rev. Lett.* **45**, 273 (1980).
- <sup>37</sup>J. L. Erskine, *Phys. Rev. Lett.* **45**, 1446 (1980).
- <sup>38</sup>D. G. Dempsey and L. Kleinman, *Phys. Rev. Lett.* **39**, 1297 (1977).
- <sup>39</sup>L. Kleinman, *Comments Solid State Phys.* **10**, 29 (1981).
- <sup>40</sup>W. Eib and F. S. Alvarado, *Phys. Rev. Lett.* **37**, 444 (1976).
- <sup>41</sup>E. Kisker, W. Gudat, M. Campagna, E. Kuhlmann, H. Hopster, and I. D. Moore, *Phys. Rev. Lett.* **43**, 966 (1979).
- <sup>42</sup>W. Gudat, E. Kisker, E. Kuhlmann, and M. Campagna, *Phys. Rev. B* **22**, 3282 (1980).
- <sup>43</sup>E. Kisker, W. Gudat, E. Kuhlmann, R. Clauberg, and M. Campagna, *Phys. Rev. Lett.* **45**, 2053 (1980).
- <sup>44</sup>I. D. Moore, and J. B. Pendry, *J. Phys. C* **11**, 4615 (1978).
- <sup>45</sup>D. S. Wang, A. J. Freeman, and H. Krakauer, *Phys. Rev. B* **26**, 1340 (1980).
- <sup>46</sup>M. Weinert, E. Wimmer, A. J. Freeman, and H. Krakauer, *Phys. Rev. Lett.* **47**, 705 (1981).
- <sup>47</sup>T. Jarlborg and A. J. Freeman, *Phys. Rev. Lett.* **45**, 653 (1980).
- <sup>48</sup>C. S. Wang and A. J. Freeman, *Phys. Rev. B* **21**, 4585 (1980).
- <sup>49</sup>O. Jepsen, J. Madsen, and O. K. Andersen, *J. Magn. Magn. Mater.* **15-18**, 867 (1980); *Phys. Rev. B* **26**, 2790 (1982).
- <sup>50</sup>H. Krakauer, M. Posternak, and A. J. Freeman, *Phys. Rev. B* **19**, 1706 (1979).
- <sup>51</sup>M. Posternak, H. Krakauer, A. J. Freeman, and D. D. Koelling, *Phys. Rev. B* **21**, 5601 (1980).
- <sup>52</sup>L. Hedin and B. I. Lundqvist, *J. Phys. C* **4**, 2064 (1971).
- <sup>53</sup>D. D. Koelling and B. N. Harmon, *J. Phys. C* **10**, 3107 (1977).
- <sup>54</sup>M. Posternak, H. Krakauer, and A. J. Freeman, *Phys. Rev. B* **25**, 755 (1982).
- <sup>55</sup>E. Wimmer, A. J. Freeman, M. Weinert, H. Krakauer, J. Hiskes, and A. M. Karo, *Phys. Rev. Lett.* **48**, 1128 (1982).
- <sup>56</sup>B. G. Baker, B. B. Johnson, and G. L. C. Maire, *Surf. Sci.* **24**, 572 (1971).
- <sup>57</sup>W. Eib and S. F. Alvarado, *Phys. Rev. Lett.* **37**, 444 (1976).
- <sup>58</sup>D. R. Hamann, *Phys. Rev. Lett.* **46**, 1227 (1981).
- <sup>59</sup>D. G. Dempsey, W. R. Grise, and L. Kleinman, *Phys. Rev. B* **18**, 1270 (1978).
- <sup>60</sup>L. Kleinman, *Phys. Rev. B* **23**, 6805 (1981).
- <sup>61</sup>J. Noffke and L. Fritsche, *J. Phys. C* **14**, 89 (1981).
- <sup>62</sup>P. J. Citrin, G. K. Wertheim, and Y. Baer, *Phys. Rev. Lett.* **41**, 1425 (1978).
- <sup>63</sup>M. C. Desjonqueres, D. Spanjaard, Y. Lassailly, and C. Guillot, *Solid State Commun.* **34**, 807 (1980).
- <sup>64</sup>A. Rosengren and B. Johansson, *Phys. Rev. B* **22**, 3706 (1980).
- <sup>65</sup>J. F. van der Veen, P. Heiman, F. J. Himpsel, and D. E. Eastman, *Solid State Commun.* **37**, 555 (1981).
- <sup>66</sup>T. M. Duc, C. Guillot, Y. Lassailly, J. Lecante, Y. Jughet, and J. C. Vedrine, *Phys. Rev. Lett.* **43**, 789 (1979).
- <sup>67</sup>P. J. Feibelman, J. A. Appelbaum, and D. R. Hamann, *Phys. Rev. B* **20**, 1433 (1979).
- <sup>68</sup>P. J. Feibelman and D. R. Hamann, *Solid State Commun.* **31**, 413 (1979).
- <sup>69</sup>J. A. Appelbaum and D. R. Hamann, *Solid State Commun.* **27**, 881 (1978).
- <sup>70</sup>J. R. Smith, F. J. Arlinghaus, and J. G. Gay, *Phys. Rev. B* **26**, 1071 (1982).
- <sup>71</sup>J. Tersoff and L. M. Falicov, *Phys. Rev. B* **26**, 1058 (1982).
- <sup>72</sup>L. Kleinman, *Phys. Rev. B* **26**, 1055 (1982).